Constructal Microdevice Manifold Design With Uniform Flow Rate Distribution by Consideration of the Tree-Branching Rule of Leonardo da Vinci and Hess–Murray Rule

Erdal Cetkin[1]
Department of Mechanical Engineering,
Izmir Institute of Technology,
Urla,
Izmir 35430, Turkey
e-mail: erdalcetkin@iyte.edu.tr

In this paper, we show how the design of a microdevice manifold should be tapered for uniform flow rate distribution. The designs based on the tree-branching rule of Leonardo da Vinci and the Hess–Murray rule were considered in addition to the constructal design. Both da Vinci and Hess–Murray designs are insensitive to the inlet velocity, and they provide better flow uniformity than the base (not tapered) design. However, the results of this paper uncover that not only pressure drop but also velocity distribution in the microdevice play an integral role in the flow uniformity. Therefore, an iterative approach was adopted with five degrees-of-freedom (inclined wall positions) and one constraint (constant distribution channel thickness) in order to uncover the constructal design which conforms the uniform flow rate distribution. In addition, the effect of slenderness of the microchannels (Svelteness) and inlet velocity on the flow rate distribution to the microchannels has been documented. This paper also uncovers that the design of a manifold should be designed with not only the consideration of pressure distribution but also dynamic pressure distribution especially for non-Svelte microdevices.
[DOI: 10.1115/1.4036089]

1 Introduction

The trend of miniaturization and advanced microelectromechanical systems (MEMS) require microdevices with uniformly distributed flows. These microdevices can be used in distinct fields such as microanalysis chips (deoxyribonucleic acid (DNA) decoding and on-site environmental monitoring systems) [1–6] and cooling [7–14]. In addition, these devices are essential for gaining advanced capabilities such as self-healing and self-cooling to engineered systems [15–18]. Vascularized structures with uniform flow rate distribution would eliminate the risk of hot spots and unhealed regions for self-cooling and self-healing applications.

Cetkin et al. [19] documented analytically that the uniform flow rate distribution and minimum pumping power requirement can be achieved with tapered channels in turbulent flow with the assumptions of Svelte designs and continuous discharge along the distributing channel. Later, Cetkin [20] showed analytically that the tapered channels also provide uniform flow rate distribution in laminar flow. He also documented the diameter profile of the distributing channel for uniform flow rate distribution with continuous discharge. Tonomura et al. [1] proposed a computational fluid dynamics (CFD)-based optimization method for plate-fin microdevices. They documented that the longer microchannels provide better flow uniformity with tapered channels and thicker collecting channel. Their automatic shape optimization procedure includes one degree-of-freedom. Later, Huang et al. [21] suggested that using two third-order polynomial functions for tapering the distributor and collecting channels in a plate-fin microdevice provides better flow uniformity than using lines. They found uniform flow rate designs for one inlet velocity (0.5 m/s) and for one Svelte design (4.5 mm microchannel length). Therefore, the literature lacks documentation of how the flow uniformity in plate-fin microdevices in non-Svelte designs for various inlet velocities can be achieved.

Constructal law stated by Adrian Bejan in 1996 [22] expresses that the flow domain should be dynamic (free to change) in order to facilitate the best performance in any time. This law has been adapted to many distinct fields such as engineering [23–27], biology [28–30], geology [31,32], and social dynamics [33,34] in order to both understand the nature and engineer the best performing designs for the given set of conditions and constraints. The current literature shows that the constructal designs are the designs with the minimum flow resistances (maximum flow accessibility) under the given constraints. For instance, the lung distributes air to a large number of alveoli (constraint) with the minimum flow resistance (objective) [35]. In addition, the constructal designs are similar to the designs seen in the nature (i.e., not biomimicry, but the designs found by the theory overlaps with the designs in the nature) [36–38].

This paper uncovers how the flow uniformity in plate-fin microdevices can be acquired for Svelte and non-Svelte designs for various inlet velocities. Two rules based on the branching thicknesses (tree-branching rule of Leonardo da Vinci and Hess–Murray rule) are considered in order to uncover the design which provides the most uniform flow rate distribution (constraint). These designs are insensitive to the inlet velocity (Hess–Murray design has one exception that the design should change when the flow regime is altered from laminar to turbulent). Later, an iterative approach based on the constructal law is adapted to uncover the design with the most uniform flow rate distribution.

2 Model

Consider the microscale manifold design shown in Fig. 1. The fluid enters from the inlet boundary, and it is distributed to the

[1]Corresponding author.

Contributed by the Heat Transfer Division of ASME for publication in the Journal of Heat Transfer. Manuscript received September 28, 2016; final manuscript received January 20, 2017; published online April 11, 2017. Assoc. Editor: Jim A. Liburdy.

five channels. Then, it is collected, and leaves the manifold from the outlet port. The width of the distributing and collecting channels is $D = 500\,\mu$m, and the height of the daughter channels and the spacing in between them are $d = 100\,\mu$m. The length of the daughter microchannels is $L = 1.5$ mm. The properties of the fluid are constant. The density and the dynamic viscosity of the fluid are $\rho = 998.2\,\text{kg/m}^3$ and $\mu = 0.001\,\text{kg/(m s)}$. The numerical solution domain is two-dimensional. The fluid flow is steady state, incompressible, and laminar. With all these in mind, the conservation of mass and momentum equations become as follows:

$$\frac{\partial u}{\partial x} + \frac{\partial v}{\partial y} = 0 \tag{1}$$

$$u\frac{\partial u}{\partial x} + v\frac{\partial u}{\partial y} = -\frac{1}{\rho}\frac{\partial P}{\partial x} + \nu\nabla^2 u \tag{2}$$

$$u\frac{\partial v}{\partial x} + v\frac{\partial v}{\partial y} = -\frac{1}{\rho}\frac{\partial P}{\partial y} + \nu\nabla^2 v \tag{3}$$

where $\nabla^2 = \partial^2/\partial x^2 + \partial^2/\partial y^2$, x and y are spatial coordinates, and u and v are the velocity components corresponding to these coordinates, respectively. P, ν, and ρ are the pressure, kinematic viscosity, and density. Fluid enters into the manifold with 1 m/s uniform velocity profile from the inlet surface of length D as shown in Fig. 1. Then the fluid is distributed to the five daughter channels of thickness d. After, the fluid moves along the channels of diameter d, and they are collected at the main collector of length scale D. Fluid exits from the main collector via outlet surface. The outlet surface is a pressure boundary condition with the gauge pressure defined as zero. The rest of the walls are defined as no slip boundaries, i.e., fluid stagnates on the wall.

The governing equations for the fluid flow were solved numerically by a finite element software [39]. The grid was nonuniform with boundary layer mesh elements in order to uncover the gradient changes near the boundaries with minimum number of mesh elements. The residual was imposed as 10^{-7} in the numerical software. Table 1 shows the ratio of the volumetric flow rate for each channel (V_i) divided by the average volumetric flow rate $(\overline{V} = \sum_1^5 V_i/5)$ relative to the number of mesh elements. Two criteria were selected for deciding that the solution is mesh independent, absolute of the relative error for the flow rate in each channel should be in the order of 10^{-3}, $|(V_i^{n+1} - V_i^n)/V_i^n| \le 10^{-3}$, and the relative error of the average flow rate calculated from the simulations in comparison with the exact value should be in the order of 10^{-3}, $|(\overline{V}^n - \overline{V}^{\text{exact}})/\overline{V}^{\text{exact}}| \le 10^{-3}$. These criteria are conformed with 43,030 number of mesh elements. Therefore, it is concluded that the numerical solutions are mesh independent.

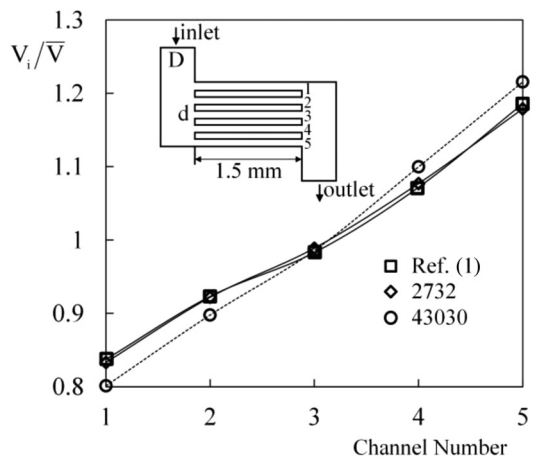

Fig. 1 Comparison of $V_i/\overline{V}$ ratio for each channel in current study and Ref. [1]

Figure 1 shows how $V_i/\overline{V}$ ratio varies for each channel as the number of mesh elements increases from 2732 to 43,030. In addition, Fig. 1 shows that the simulation results of the current study with 2732 number of mesh elements are in good agreement with the numerical study results of Ref. [1], i.e., the maximum relative error is 0.79%, which corresponds to the channel number of 5. However, Table 1 shows that the 43,030 number of mesh elements do not only demonstrate mesh independency but also conforms the accurate average flow rate calculations. Therefore, even though the 2732 number of mesh elements yield almost the same results with the results of Ref. [1], it is decided to use finer mesh elements in the current study.

3 Non-Svelte Manifolds

Achieving the uniformity in fluid distribution is more complex in non-Svelte manifolds rather than Svelte ones. In Svelte manifolds, the majority of the pressure drop is due to continuous channels as shown in Ref. [40]. For instance, Fig. 1.2 of Ref. [40] shows that the pressure drop due to the local losses decreases less than 5% when Svelteness is greater than 10 and 50 for fully developed laminar and turbulent ($f = 0.01$) flows. Therefore, the effect of local losses due to the distribution diminishes as a manifold becomes slender (as Svelteness increase). Here, we uncover how the uniform distribution of a fluid stream in a non-Svelte manifold can be achieved.

Consider the non-Svelte manifold design of Fig. 1. However, the shape of the main distributing and collecting channels is no longer constant, i.e., varies along the flow direction. Literature shows how tapering a channel would enable the uniform fluid discharge along the channel [19,20]. However, it should be noted that there are five channels in which fluid is distributed and collected, i.e., the flow discharge along the distributor channel is not continuous. Therefore, there are designs which would provide better flow uniformity than the tapered designs mentioned in the literature.

First, the collecting and distributing channels are tapered by using the tree-branching rule of Leonardo da Vinci [41,42]. Leonardo da Vinci considered that the summation of the cross sections of the branches at any height should be equal to the thickness of the trunk. Therefore, if there is a new branch attached to the distributor channel, then the thickness of the main distributing channel should be decreased with that amount. Likewise, if a branch is connected to the collector channel, the thickness of the collector should increase with the same amount. The manifold design in Fig. 2(*a*) represents how the non-Svelte manifold of Fig. 1 was altered by using the da Vinci's branching rule. Note that the change in the cross section is not sudden but along the thickness of the microchannel with inclined walls of 45 deg as shown in Fig. 2(*a*). The reason for that is in order to mimic if the smallest branch is a fiber with a given thickness, i.e., there should be a curvature where the fiber is bending as it is leaving from the main branch. This transitional change in the cross section is also used for eliminating sudden changes in the pressure and directing the fluid to the channels. Figure 2 shows that the maximum deviation of flow rate in each channel divided by the average flow rate becomes at least 10% better in comparison with the performance of manifold design of Fig. 1 by using the branching rule of da Vinci. Figure 2(*b*) also shows how the volumetric flow rate over the averaged volumetric flow rate for each channel varies when only main distributing or collecting channel cross sections were varied by using the branching rule. In addition, Fig. 2(*b*) shows that tapering only the distributing channel would yield the same flow rate uniformity with tapering both collecting and distributing channels. However, tapering only the collecting channel results in worse flow uniformity than the all the other designs including the design of Fig. 1. This result is reasonable because the flow rate is minimum at the channel 1 and it increases from 1 to 5 in the base

Table 1 Ratio of the volumetric flow rate for each channel over the average flow rate relative to the number of mesh elements

	$V_i/\overline{V}$ ratio corresponding to the number of mesh elements					
Channel number	2732	3984	6394	16,058	43,030	47,340
1	0.833161	0.830804	0.818880	0.808809	0.801220	0.800886
2	0.922030	0.908492	0.905058	0.901372	0.897845	0.897290
3	0.988936	0.978209	0.985329	0.986181	0.985651	0.985736
4	1.077002	1.077012	1.092894	1.096498	1.099770	1.099272
5	1.178868	1.205481	1.197837	1.207138	1.215512	1.216813
$\overline{V}(\mathrm{m}^2/\mathrm{s})$	9.23×10^{-5}	9.60×10^{-5}	9.78×10^{-5}	9.95×10^{-5}	1.00×10^{-4}	1.00×10^{-4}
$\lvert(\overline{V}^n - \overline{V}^{\mathrm{exact}})/\overline{V}^{\mathrm{exact}}\rvert$	0.0774	0.0405	0.0219	0.0050	0.0016	0.0017

design of Fig. 1. This shows that the flow resistances are decreasing from channels 1 to 5. Tapering only the collecting channel increases the flow resistances for channels where it is already high (channels 1 and 2) and decreases the flow resistances where it is low (channel 4 and 5). Therefore, the difference of the pressure drop values for each channel increases, and so is the flow nonuniformity.

Next, consider the same tapering concept by using Hess–Murray rule. The thickness of the distributing channel is decreased at the junction of each branch. Therefore, the distributing channel thickness varies nonuniformly. d_i represents the decrease in the thickness of the distributed channel connected to each microchannel, i.e., subindices of i correspond to the channel numbers as shown in Fig. 3(*a*). Similar to the branching rule of da Vinci, the distributing channel is tapered with inclined walls.

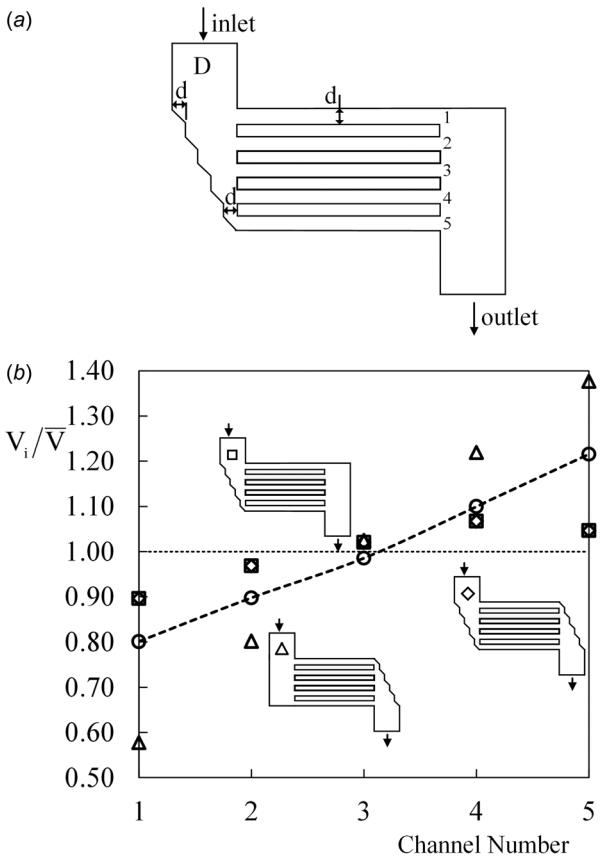

Fig. 2 (*a*) Geometry of the manifold with tapered distributing channel with the branching rule of da Vinci and (*b*) flow rate in each channel divided by the average flow rate for tapered collecting channel (triangle), tapered distributing channel (square), and tapered distributing and collecting channels (diamond), and nontapered design of Fig. 1 (circle) with 1.5-mm microchannel length and 1 m/s inlet velocity

However, the slope of walls varies based on the thickness of the distributing channel.

Hess–Murray rule uncovers how the diameter ratio at the junctions should be when a mother tube gives birth to n number of daughter tubes in order to minimize the flow resistances. However, in the current study new branches appear one by one along the distributing channel. Therefore, the diameter ratio at the junctions is not expected to be $2^{1/3}$ as it is documented in the literature when one mother tube gives birth to two identical daughter tubes [40]. Therefore, the effect of this thickness ratio should also be documented.

Figure 3 documents flow rate value of the each channel divided by the average flow rate value when the diameter ratio at the junctions varies based on the Hess–Murray rule. In addition, only the distributing channel is tapered as shown in Fig. 2 that tapering both the distributing and collecting channels in da Vinci design provided the same flow rate distribution in microchannels. All the diameter ratios correspond better flow uniformity in comparison with the nontapered design of Fig. 1. However, the difference in the flow rate of each channel in comparison with the average flow rate decreases from 17% to 5% as the diameter ratio is decreased from $2^{1/3}$ to $2^{1/6}$. In addition, Fig. 3 shows that the flow rate at channels 1 and 2 increases as the diameter ratio is big such as $2^{1/3}$, and the flow rates of channels 1 and 2 become in the same order of channels 5 and 4, respectively, as this ratio decreases to $2^{1/6}$. Figure 3 also shows that the flow rate at channel 4 and 5 increases as the flow rate of channels 1 and 2 decreases. Decreasing the diameter ratio from $2^{1/6}$ to $2^{1/7}$ increases the maximum deviation $(|(\overline{V} - V_{\max})|/\overline{V})$ of the flow rate.

Figures 2 and 3 show that the designs altered with branching rule of Leonardo da Vinci and Hess–Murray rule provide better flow uniformity in comparison with the base design of Fig. 1. However, the flow rate in each channel is maximum 5% different than the average flow rate in both da Vinci and Hess–Murray designs. Constructal law suggests that the design should be freely morphed in order to achieve minimum flow resistances. da Vinci and Hess–Murray designs uncovered that tapering the distribution channel with inclined walls provides better flow uniformity in microdevice channels. Combining the constructal approach with the results of da Vinci and Hess–Murray designs suggest that inclined walls which can be freely morphed may uncover the design which has the best flow uniformity. Therefore, an iterative approach based on the constructal law is adapted. The positions of the inclined walls are freely changed with the constraint of they should stay in the predefined distribution channel thickness ($D = 500\,\mu$m), i.e., five degrees-of-freedom and one constraint. The thickness of the distributor at the junctions each microchannel is decreased or increased depending on whether the flow rate is greater or smaller than the average flow rate. Maximum 1% error in between the average flow rate and the individual channel flow rates was dictated as the ending criterion of the iterations. After ten iterations, the design with maximum 0.8% relative flow rate difference was found, which is shown and drawn in scale in Fig. 4. Figure 4 shows the summary of flow rate distribution of the four competing designs for 1.5 mm microchannel length and inlet velocities of 0.5, 1, and 2 m/s. Both da Vinci and

Hess–Murray designs performs better than the base design. However, when the inlet velocity is 0.5 m/s, Hess–Murray design provides 1% better flow uniformity, i.e., the maximum deviation in the flow rate ($(|(\overline{V} - V_{max})|/\overline{V})$ is 1% smaller in Hess–Murray design than the da Vinci design. Constructal design performs the best (maximum deviation of flow rate in each channel is the minimum) in comparison with the all other designs. In addition, the selected error margin can be decreased and a design with lower maximum deviation of flow rate in each channel can also be found depending on the application. Constructal design of Fig. 4 shows that the thickness of the distributing channel should suddenly decrease at first and then the change in the thickness becomes smoother unlike in da Vinci and Hess–Murray designs.

Inlet velocity also affects the flow rate distribution to each microchannel. As the inlet velocity decreases, the flow rate distribution becomes more uniform in the base design, i.e., the maximum deviation of the flow rate decreases to 13% from 20%. Similarly, this deviation in da Vinci and Hess–Murray designs increases 2% and 3%, respectively. Even though the constructal design also provides the minimum of this maximum deviation in 0.5 m/s velocity, it is 2% different than the exact value of the average velocity. However, it should be noted that the constructal design was iteratively found for 1.5-mm microchannel length and 1 m/s velocity. Therefore, change in the performance is expected as these parameters change. In addition, a new constructal design should be iteratively found for each inlet velocity and microchannel length scale. For the sake of simplicity, the constructal design of Fig. 4 is labeled as the constructal design except it is specified. It should also be noted a better performing design could be found for each set of design criteria by following the same iterative approach.

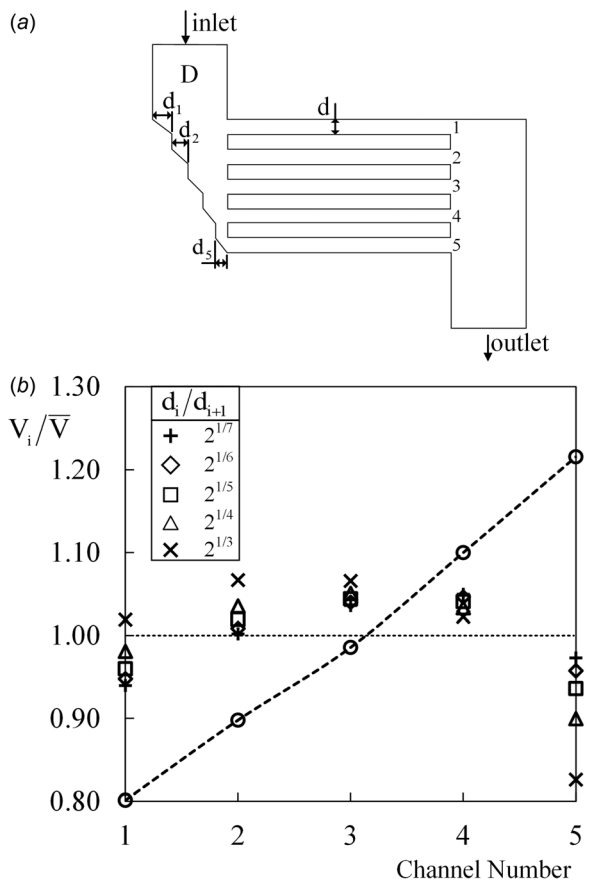

Fig. 3 (*a*) Geometry of the manifold with tapered distributing channel with Hess–Murray rule and (*b*) flow rate in each channel divided by the average flow rate for tapered distributing channel with 1.5-mm microchannel length and 1 m/s inlet velocity

In addition, Fig. 4 also shows how the flow rate in each microchannel is affected when the inlet velocity is increased from 1 m/s to 2 m/s. Flow nonuniformity in microchannel increases for each design as the inlet velocity increases. The maximum deviation in the flow rate in comparison with the average flow rate becomes 30%, 14%, 8%, and 6% for the base, da Vinci, Hess–Murray, and constructal designs with 2 m/s inlet velocity, respectively. Figure 5 shows how the summation of the deviations in each channels and the maximum deviations vary for the competing designs with (a) 0.5 m/s, (b) 1 m/s, and (c) 2 m/s inlet velocities. The maximum deviation and the summation of the resistances are the smallest with constructal design. This result shows that even the

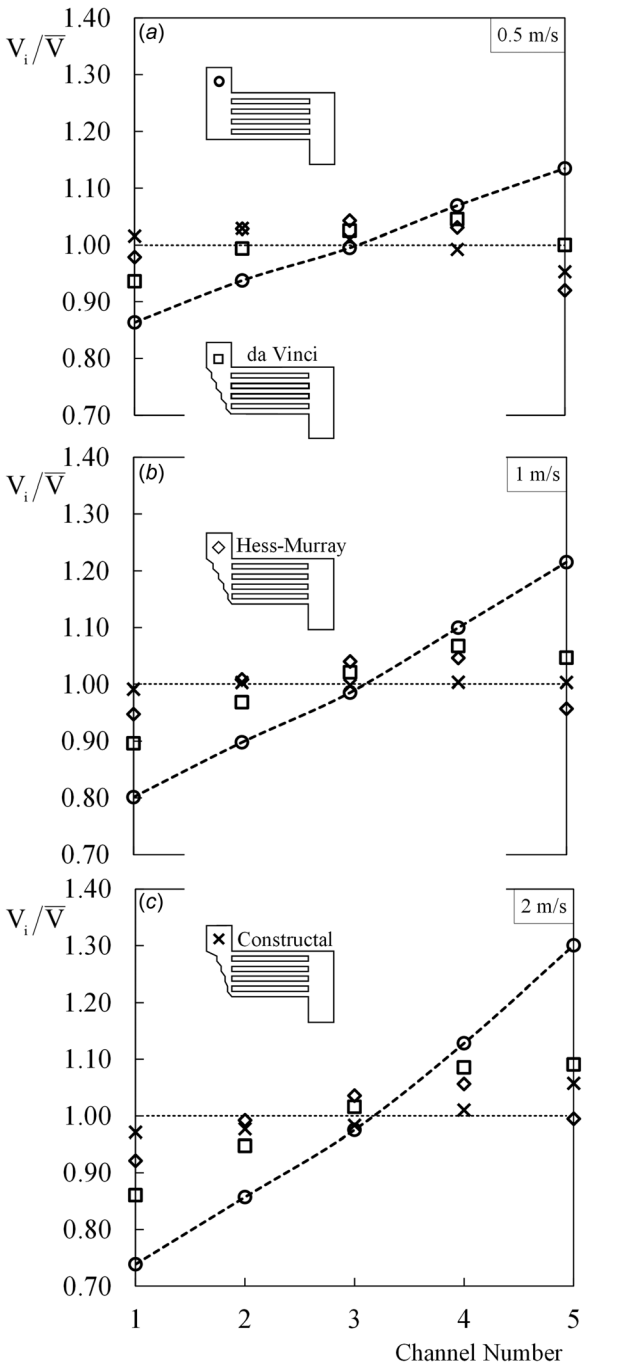

Fig. 4 Flow rate in each channel divided by the average flow rate for four competing designs: design of Fig. 1 (circle), da Vinci (square), Hess–Murray with $2^{1/6}$ thickness ratio (diamond), and constructal design (cross) with the inlet velocities of (*a*) 0.5 m/s, (*b*) 1 m/s, and (*c*) 2 m/s

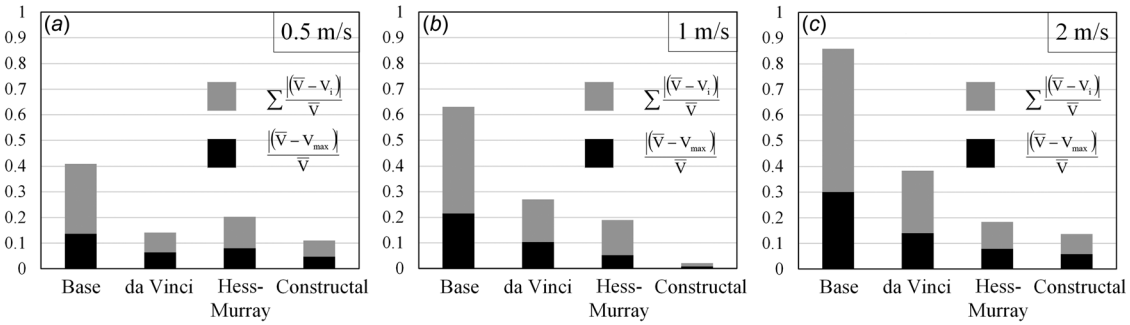

Fig. 5 Sum of the deviations and maximum deviations for the competing designs with the inlet velocities of (*a*) 0.5 m/s, (*b*) 1 m/s, and (*c*) 2 m/s

constructal design was iteratively found for 1 m/s inlet velocity, it provides the best flow rate uniformity (minimum of the maximum deviation) in comparison with the other competing designs. In addition, Fig. 5 shows that the maximum deviation is smaller in da Vinci design than the Hess–Murray design with 0.5 m/s. Furthermore, Fig. 5 shows that the design of manifold is a function of inlet velocity for uniform distribution of the fluid. Therefore, unlike in the literature, not only pressure distribution should be considered for flow uniformity [1,19–21].

4 Svelte Manifolds

Consider the microdevice shown in Fig. 1 with longer microchannel lengths 4.5 and 13. 5 mm instead of 1.5 mm. The microchannels become slender (Svelte) as the length scale increases while its thickness (or diameter) is constant. Therefore, the continuous pressure drop along the microchannels increases greatly, and the pressure drop at the junctions becomes negligibly small in comparison with the continuous pressure drop as the designs become slender. This indicates that the effect of local pressure drop diminishes as the design becomes slender, and the manifold design effect on the flow uniformity also diminishes. The current literature only uncovers how the manifold shape should be for Svelte microdevices for limited inlet velocities, i.e., Ref. [21] only considers 0.5 m/s inlet velocity. The best designs in the literature also includes increased thickness for the collecting channel; therefore, their surface area is greater than the designs mentioned in the current study.

Figure 6 shows how the flow rate along each channel divided by the average flow rate varies for four competing designs introduced in Fig. 4 when the microchannel length scale is 4.5 mm. Figure 6(*a*) documents the flow rates when the inlet velocity is 0.5 m/s. Similar to Figs. 4 and 5, the base design performs the worst and the constructal design performs the best in terms of uniform distribution of flow rate. In addition, Figs. 6(*b*) and 6(*c*) shows how the flow rate is distributed along microchannels when the inlet fluid velocity is 1 and 2 m/s. Similar to Fig. 6(*a*), Figs. 6(*b*) and 6(*c*) also show that the flow uniformity increases as the design is altered from the base design to the constructal design. Both da Vinci and Hess–Murray designs perform better than the base design but worse than the constructal design in terms of flow uniformity. Comparison of Figs. 6(*a*)–6(*c*) shows that the constructal design provides better flow uniformity when the inlet velocity is 1 m/s. This is expected because the constructal design was iteratively found for 1.5-mm microchannel length scale and 1 m/s inlet velocity.

Huang et al. [21] shows that when the microchannel length scale is 4.5 mm and inlet velocity is 0.5 m/s, better flow uniformity can be achieved than the designs mentioned in Fig. 6(*a*). However, the results of the non-Svelte manifolds uncover that if the constructal approach is implemented for 4.5-mm microchannel length scale and 0.5 m/s inlet velocity, better flow uniformity can be found with the designs of smaller surface area. In order to show the correctness of this result, the constructal design of Fig. 4 was selected as the initial design for iterative optimization with 4.5-mm microchannel length scale and 0.5 m/s inlet velocity as dictated in Ref. [21]. The iterative procedure is the same in Sec. 3 with only exception of error criterion was altered from 1% to 0.1%. Because the initial design is the constructal design for 1.5-mm microchannel length scale and 1 m/s inlet velocity, the constructal design was found after four iterations. Figure 7 shows the flow rate values divided by the average flow rates along the each channel for three designs: Type B-O and Type OPT1 of Ref. [21] and the constructal design. Both Type B-O and OPT1 provides better flow uniformity in channels labeled with 2, 3, and 5 than in channels 1 and 4. However, the iteratively found constructal design provides the almost same flow rate (0.1% error margin) for the each channel. The constructal design not only provides better flow uniformity but also provides a design with smaller surface area than in the designs of Refs. [1] and [21], i.e., the collecting channel of the designs of Refs. [1] and [21] is 500 μm thicker than the constructal design.

Figure 8 shows how the flow rate in each channel varies for four competing designs (base, da Vinci, Hess–Murray, and constructal design iteratively found for 1.5-mm microchannel length and 1 m/s inlet velocity) when the microchannel length is 13.5 mm and the inlet velocity is (a) 0.5 m/s, (b) 1 m/s, and (c) 2 m/s. Figure 8 shows that tapered distributing channel designs (da Vinci, Hess–Murray, and constructal) provides better flow uniformity for all the inlet velocities. Figure 8(*a*) shows that the flow uniformity is the best with the constructal design, which provides 0.2% better flow uniformity than the Hess–Murray design. Figures 8(*b*) and 8(*c*) show that the Hess–Murray design provides better flow uniformity than the constructal design (0.1% and 0.2%, respectively). However, it should be noted that the constructal design was found iteratively for 1.5 mm microchannel length and 1 m/s inlet velocity. Therefore, there is a constructal design that performs better than all the other designs if the design is freely morphed for 13.5 mm microchannel length and corresponding inlet velocity as shown in Fig. 7. In addition, as the effect of local pressure drop diminishes the effect of velocity profile on the flow uniformity becomes evident.

Comparison of Figs. 6 and 8 shows that the flow nonuniformity decreases as the microchannels become slender (Svelteness increases) as expected. Bejan and Lorente [40] show that as the Svelteness increases the effect of local pressure drops diminishes. Figure 9 confirms this result as the maximum flow rate deviation decreases in base design from 30% to 17% and 5% as the microchannel length increases from 1.5 mm to 4.5 mm and 13.5 mm, respectively. Figure 9 documents the maximum deviation in the flow rate for base and constructal designs which correspond to the maximum and minimum values, respectively, in between all the competing designs.

In order to uncover the effect of velocity distribution consider the design of Fig. 10(*a*) where five ducts with the same length scale and thickness are connected to the inlet and outlet ports.

Each duct yields the same pressure drop in between its inlet and outlet sections because the length and the thickness of the channels are identical. Therefore, if the pressure drop is the sole effecting parameter, the flow rate along the each duct should be the same. Figure 10(*b*) shows the flow rate along the each channel divided by the average velocity when the microchannel length scale is 1.5 mm and inlet velocity is 1 m/s in comparison with the base design and the constructal design. Figure 10(*b*) shows that even the pressure drop along the microchannels in Fig. 10(*a*) is identical, but the flow rate in each channel is not. The flow rate distribution is more uniform in the constructal design than in the design of Fig. 10(*a*). This shows that the pressure distribution is not the only parameter in consideration of the flow uniformity.

Figure 11 shows the velocity, pressure, and overall pressure contours of three designs: the designs of Figs. 1, 4, and 10(*a*). Velocity distributions show that the constructal design and the design of Fig. 10(*a*) provide almost uniform flow rate across each channel unlike in the base design case. The constructal design shows sudden velocity increases due to the inclined walls; however, the most uniform flow rate distribution is achieved with the constructal design (i.e., the maximum deviation of $V_i/\overline{V}$ ratio is the smallest with the constructal design) as shown in Fig. 10(*b*). Distribution of pressure is the most uniform with the design of Fig. 10(*a*). Figure 11 also confirms that this design provides constant pressure drop along each channel. In addition, constructal design provides more uniform pressure distribution than the base design. Last but not least, Fig. 11 shows how overall pressure (summation of static and dynamic pressures as in Bernoulli's equation, note that the pressure related with potential difference is negligibly small due to the length scale of the microdevice) is distributed for each design. Overall pressure is calculated as the summation of the static pressure and the dynamic pressure ($\rho U^2/2$, where U is the local velocity magnitude). Overall pressure distribution of the design of Fig. 10(*a*) is almost uniform. Channels of number 1 and 5 show slightly thinner and longer region with greater overall pressure value at the outlet boundary. Figure 10(*b*) also shows that the flow rates in channels 1 and 5 is 1% and 2% less than the average flow rate value, respectively. The outlet boundary is essential because the flow rate is the function of pressure drop along each streamline. Therefore, not only at the connection with the collecting channel but also the pressure drop along the connecting channel should be considered. Commenting on the overall pressure distribution on the designs of Figs. 1 and 4 is complicated due to the overlapped streamlines. However, it is obvious that the overall pressure value is more uniform in the constructal design in comparison with the base design. Furthermore, it is expected to have greater overall pressure value where the channel 1 is connected to the collecting channel than the location where the channel 5 is connected to it because the fluid flowing in channel 1 moves on a longer path in the collecting channel. This increases the pressure drop of fluid flowing in channel 1. Therefore, the overall pressure values should be the same at the same distance from the inlet boundary for the streamlines of the fluid flowing in microchannels in order to have uniform fluid distribution. For instance, the overall pressure value of channel 1 at the connection of the collecting channel is almost the same (3% fluctuation, which is acceptable because the length of the each

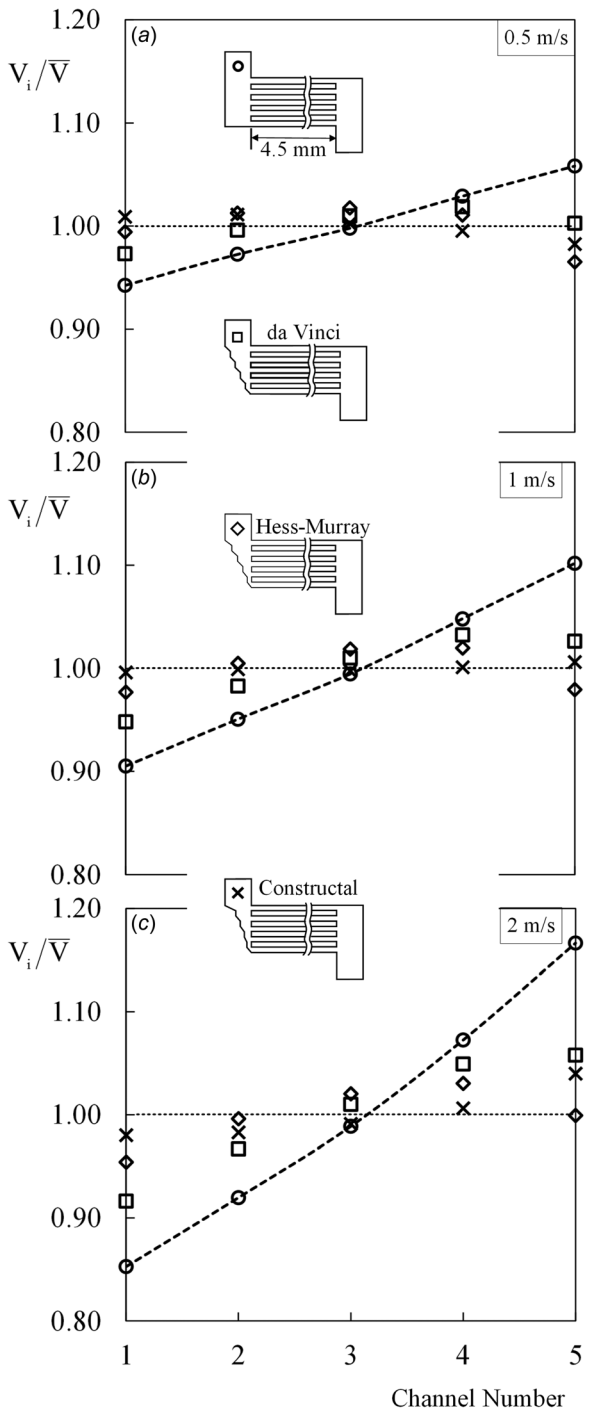

Fig. 6 Flow rate in each channel divided by the average flow rate for four competing designs with inlet velocities of (*a*) 0.5 m/s, (*b*) 1 m/s, and (*c*) 2 m/s

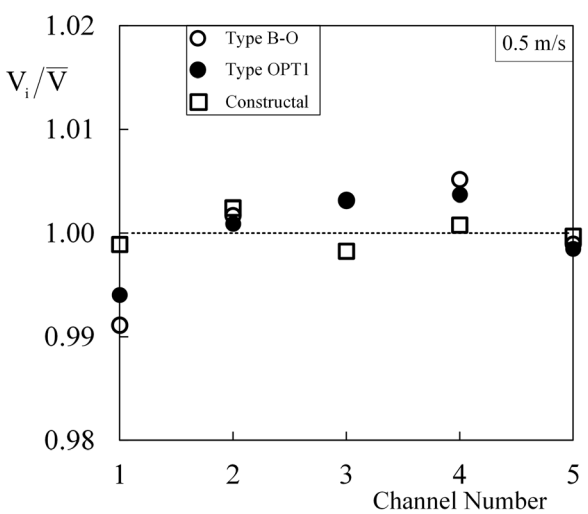

Fig. 7 Flow rate in each channel divided by the average flow rate for three competing designs: Type B-O and Type OPT1 of Ref. [21] and the constructal design

streamline has been approximated) with the overall pressure value of channel 5 at 700 μm after it is connected to the distributing channel. Therefore, it can be concluded that the overall pressure distribution governs the flow rate distribution rather than sole consideration of the pressure distribution. However, that does not mean the constraint should be the overall pressure drop in between inlet and outlet boundaries. Unlike, this indicates that if the overall pressure drop along each stream becomes the same, then the distribution of fluid would expected to be more uniform, which is in accordance with Bernoulli's equation. In addition, pressure drop is the smallest with the base design as shown in Fig. 11. However, it should be noted that the objective is to distribute the fluid homogeneously to the microchannels. Constructal design conforms this objective as shown in Fig. 10(*b*), and it requires smaller pressure drop than the design of Fig. 10 as can be seen in Fig. 11.

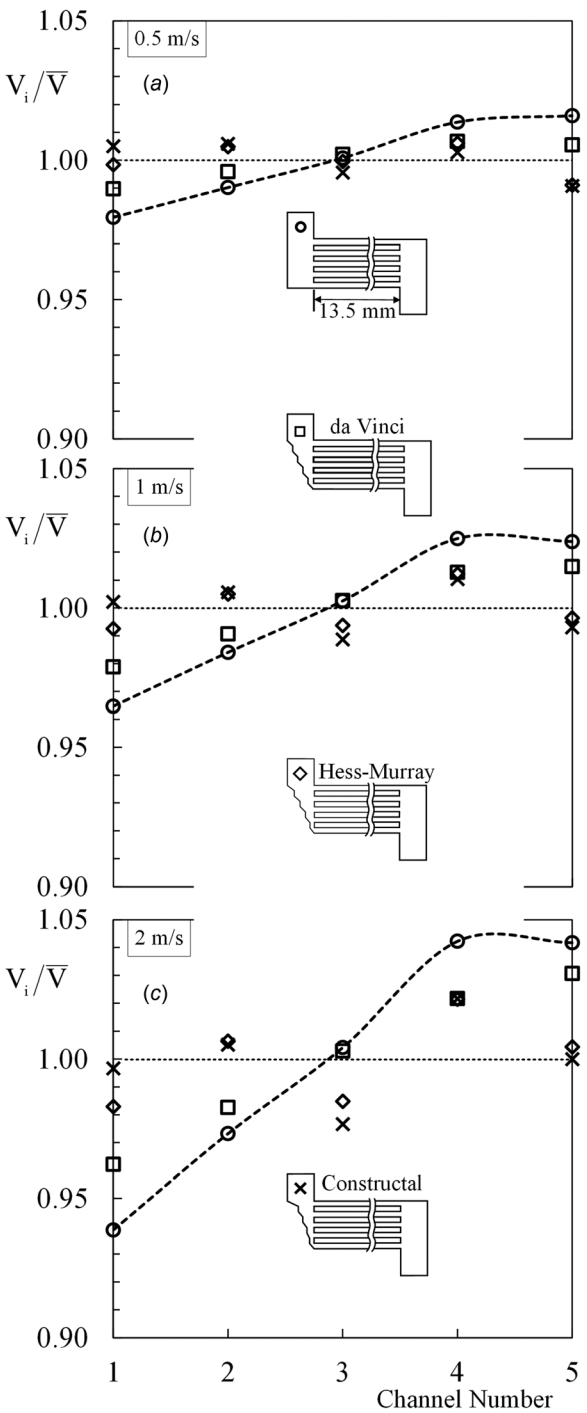

Fig. 8 Flow rate in each channel divided by the average flow rate for four competing designs when the microchannel length is 13.5 mm with inlet velocities of (*a*) 0.5 m/s, (*b*) 1 m/s, and (*c*) 2 m/s

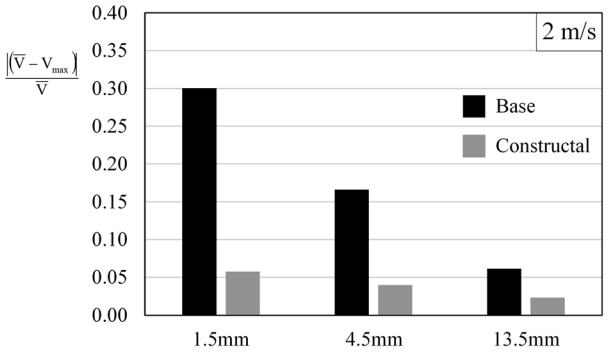

Fig. 9 Maximum deviation of the designs with maximum (base) and minimum deviations (constructal) with 2 m/s inlet velocity for length of channels of 1.5 mm, 4.5 mm, and 13.5 mm

5 Conclusions

This paper shows that there is a constructal manifold design for each microchannel length and inlet velocity. This constructal design provides better flow uniformity than other competing

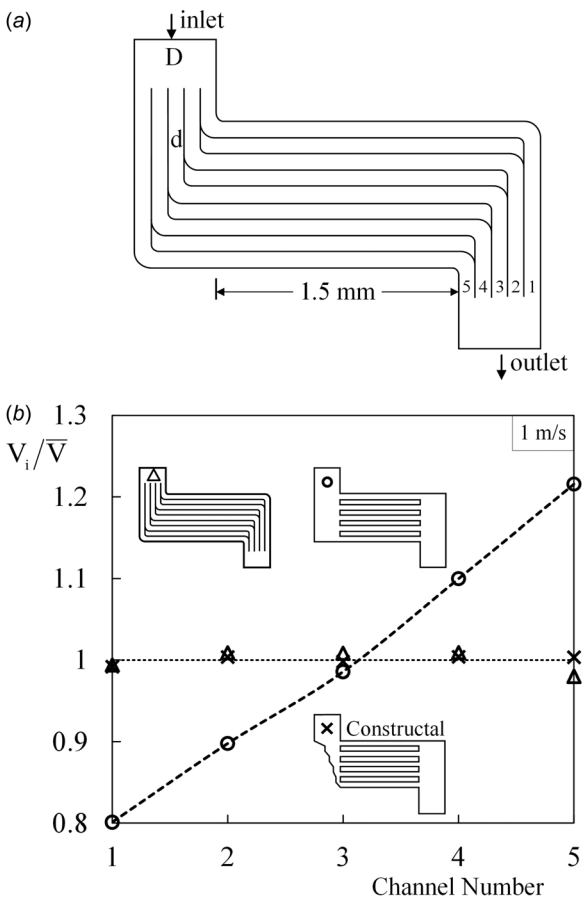

Fig. 10 (*a*) Geometry of a manifold with 5 identical length microchannels and (*b*) flow rate in each channel divided by the average flow rate for the base design, the constructal design, and the design of Fig. 10(*a*) with 1.5-mm microchannel length and 1 m/s inlet velocity

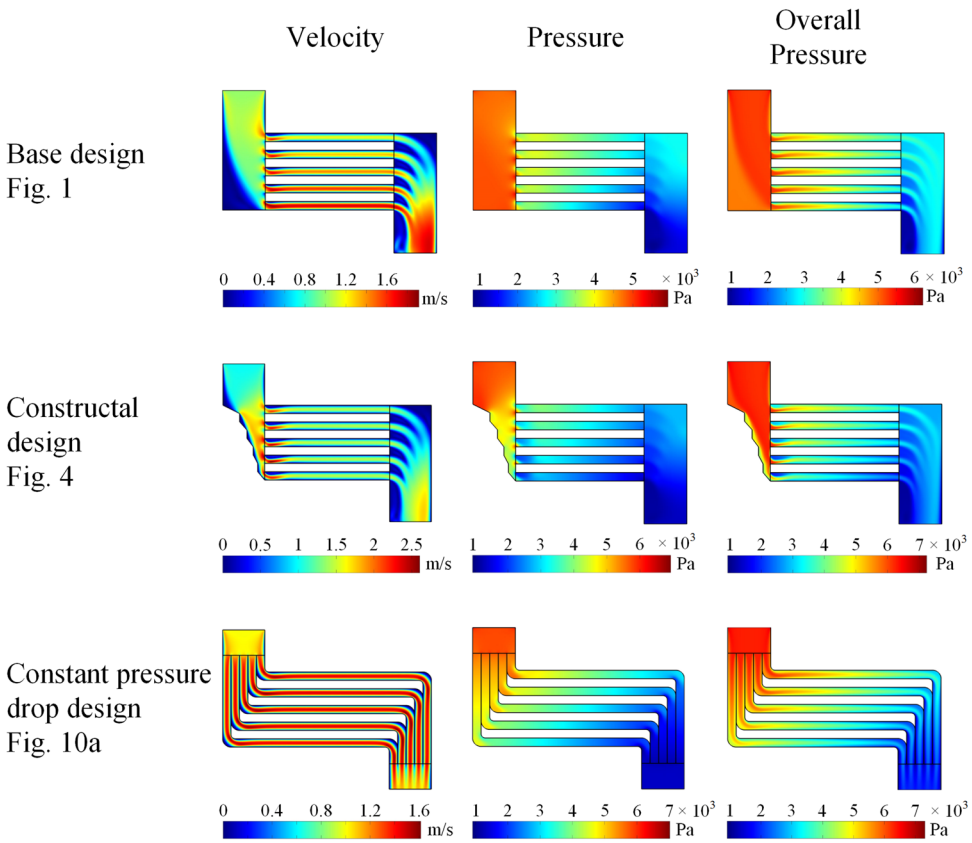

Fig. 11 Velocity, pressure, and overall pressure (summation of static and dynamic pressures) contours of the designs of Figs. 1, 4, and 10(*a*) with 1 m/s inlet velocity

designs, and it is also more compact (smaller surface area) than the others. In addition, this paper documents the flow rate uniformity in each microchannel for competing designs such as da Vinci and Hess–Murray which are based on branching rules for trees and the constructal design which is based on the minimization of the flow resistances with freely morphed designs. Both da Vinci and Hess–Murray designs are superior to the base design; however, they do not correspond to the desired flow uniformity. These designs are static, i.e., they are not a function of inlet velocity, and they are a good reference points as the initial designs of the constructal design iteration procedure.

Furthermore, both Svelte and non-Svelte microdevice manifolds were considered in order to uncover the effect of pressure and velocity distributions on the flow rate distribution to each microchannel. The effect of local pressure drops in Svelte manifolds becomes negligibly small as Svelteness increases, which is not the case in the non-Svelte manifolds. Therefore, as the Svelteness of a manifold increases the effect of design on the flow uniformity decreases especially in low velocity magnitudes such as 0.5 m/s. However, the results showed that not only static pressure but also dynamic pressure plays an integral role in the uniform flow rate distribution in a manifold (both in Svelte and non-Svelte manifolds).

Acknowledgment

This work was supported by the Scientific and Technological Research Council of Turkey (TUBITAK) under Grant No. 114M592.

Nomenclature

d = height of the microchannels, μm
D = width of the distributing and collecting channels, μm
f = friction factor
L = length of the microchannels, μm
P = pressure, N·m^{-2}
u, v = velocity components, m s^{-1}
U = local velocity magnitude, m s^{-1}
V = volumetric flow rate per unit length, m^2 s^{-1}
x, y = spatial coordinates, m

Greek Symbols

μ = dynamic viscosity, kg m^{-1} s^{-1}
ν = kinematic viscosity, m^2 s^{-1}
ρ = density, kg m^{-3}

Subscript

i = index

Superscripts

exact = exact
n = index of the mesh independency test
$\bar{}$ = average

References

[1] Tonomura, O., Tanaka, S., Noda, M., Kano, M., Hasebe, S., and Hashimoto, I., 2004, "CFD-Based Optimal Design of Manifold in Plate-Fin Microdevices," Chem. Eng. J., **101**(1–3), pp. 397–402.
[2] Lagally, E. T., Medintz, I., and Mathies, R. A., 2001, "Single-Molecule DNA Amplification and Analysis in an Integrated Microfluidic Device," Anal. Chem., **73**(3), pp. 565–570.
[3] Sanders, G. H. W., and Manz, A., 2000, "Chip-Based Microsystems for Genomic and Proteomic Analysis," TrAC, **19**(6), pp. 364–378.
[4] Lee, D., Kim, Y. T., Jee, J. W., Kim, D. H., and Seo, T. S., 2016, "An Integrated Direct Loop-Mediated Isothermal Amplification Microdevice Incorporated With an Immunochromatographic Strip for Bacteria Detection in Human Whole Blood and Milk Without Sample Preparation Step," Biosens. Bioelectron., **79**, pp. 273–279.

[5] Sweeney, J., Whitney, C., and Wilson, C. G., 2009, "A Plasma Spectroscopic Microdevice for On-Site Water Monitoring," IEEE Sensors, Vol. 1–3, pp. 2005–2008.
[6] Sanchez, Z., Tani, A., Suzuki, N., Kariyama, R., Kumon, H., and Kimbara, K., 2013, "Assessment of Change in Biofilm Architecture by Nutrient Concentration Using a Multichannel Microdevice Flow System," J. Biosci. Bioeng., **115**(3), pp. 326–331.
[7] Xie, Y., Shen, Z., Zhang, D., and Lan, J., 2014, "Thermal Performance of a Water-Cooled Microchannel Heat Sink With Grooves and Obstacles," ASME J. Electron. Packag., **136**(2), p. 021001.
[8] Wibel, W., Schygulla, U., and Brandner, J. J., 2011, "Micro Device for Liquid Cooling by Evaporation of R134a," Chem. Eng. J., **167**(2–3), pp. 705–712.
[9] Xia, G. D., Jiang, J., Zhai, Y. L., and Ma, D. D., 2015, "Effects of Different Geometric Structures on Fluid Flow and Heat Transfer Performance in Microchannel Heat Sinks," Int. J. Heat Mass Transfer, **80**, pp. 439–447.
[10] Bello-Ochende, T., Liebenberg, L., and Meyer, J. P., 2007, "Constructal Cooling Channels for Micro-Channel Heat Sinks," Int. J. Heat Mass Transfer, **50**(21–22), pp. 4141–4150.
[11] Kosar, A., and Peles, Y., 2005, "Thermal-Hydraulic Performance of MEMS-Based Pin Fin Heat Sink," ASME J. Heat Transfer, **128**(2), pp. 121–131.
[12] Lee, Y. J., Lee, P. S., and Chou, S. K., 2013, "Numerical Study of Fluid Flow and Heat Transfer in the Enhanced Microchannel With Oblique Fins," ASME J. Heat Transfer, **135**(4), p. 041901.
[13] Khan, M. G., and Fartaj, A., 2011, "Heat Exchanger: A Review on Microchannel Heat Exchangers and Potential Applications," Int. J. Energy Res., **35**(7), pp. 553–582.
[14] Wei, X., Joshi, Y., and Patterson, M. K., 2007, "Experimental and Numerical Study of a Stacked Microchannel Heat Sink for Liquid Cooling of Microelectronic Devices," ASME J. Heat Transfer, **129**(10), pp. 1432–1444.
[15] Toohey, K. S., Sottos, N. R., Lewis, J. A., Moore, J. S., and White, S. R., 2007, "Self-Healing Materials With Microvascular Networks," Nat. Mater., **6**(8), pp. 581–585.
[16] White, S. R., Sottos, N. R., Geubelle, P. H., Moore, J. S., Kessler, M. R., Sriram, S. R., Brown, E. N., and Viswanathan, S., 2001, "Autonomic Healing of Polymer Composites," Nature, **409**(6822), pp. 794–797.
[17] Cetkin, E., 2015, "Constructal Vascular Structures With High-Conductivity Inserts for Self-Cooling," ASME J. Heat Transfer, **137**(11), p. 111901.
[18] Yenigun, O., and Cetkin, E., 2016, "Experimental and Numerical Investigation of Constructal Vascular Channels for Self-Cooling: Parallel Channels, Tree-Shaped and Hybrid Designs," Int. J. Heat Mass Transfer, **103**, pp. 1155–1165.
[19] Cetkin, E., Lorente, S., and Bejan, A., 2010, "Natural Constructal Emergence of Vascular Design With Turbulent Flow," J. Appl. Phys., **107**(11), p. 114901.
[20] Cetkin, E., 2014, "Emergence of Tapered Ducts in Vascular Designs With Laminar and Turbulent Flows," J. Porous Media, **17**(8), pp. 715–722.
[21] Huang, C.-H., Wang, C.-H., and Kim, S., 2016, "A Manifold Design Problem for a Plate-Fin Microdevice to Maximize the Flow Uniformity of System," Int. J. Heat Mass Transfer, **95**, pp. 22–34.
[22] Bejan, A., 1997, *Advanced Engineering Thermodynamics*, 2nd ed., Wiley, New York.
[23] Lorenzini, G., Machado, B. S., Isoldi, L. A., dos Santos, E. D., and Rocha, L. A. O., 2016, "Constructal Design of Rectangular Fin Intruded Into Mixed Convective Lid-Driven Cavity Flows," ASME J. Heat Transfer, **138**(10), p. 102501.
[24] Bejan, A., 2015, "Constructal Law: Optimization as Design Evolution," ASME J. Heat Transfer, **137**(6), p. 061003.
[25] Rocha, L. A. O., Lorente, S., and Bejan, A., 2002, "Constructal Design for Cooling a Disc-Shaped Area by Conduction," Int. J. Heat Mass Transfer, **45**(8), pp. 1643–1652.
[26] Muzychka, Y. S., 2005, "Constructal Design of Forced Convection Cooled Microchannel Heat Sinks and Heat Exchangers," Int. J. Heat Mass Transfer, **48**(15), pp. 3119–3127.
[27] Azoumah, Y., Neveu, P., and Mazet, N., 2007, "Optimal Design of Thermochemical Reactors Based on Constructal Approach," AIChe J., **53**(5), pp. 1257–1266.
[28] Miguel, A. F., 2006, "Constructal Pattern Formation in Stony Corals, Bacterial Colonies and Plant Roots Under Different Hydrodynamics Conditions," J. Theor. Biol., **242**(4), pp. 954–961.
[29] Bejan, A., Lorente, S., and Lee, J., 2008, "Unifying Constructal Theory of Tree Roots, Canopies and Forests," J. Theor. Biol., **254**(3), pp. 529–540.
[30] Lucia, U., Ponzetto, A., and Deisboeck, T. S., 2014, "A Thermo-Physical Analysis of the Proton Pump Vacuolar-ATPase: The Constructal Approach," Sci. Rep., **4**, p. 6763.
[31] Reis, A. H., 2006, "Constructal View of Scaling Laws of River Basins," Geomorphology, **78**(3–4), pp. 201–206.
[32] Bejan, A., 2007, "Constructal Theory of Pattern Formation," Hydrol. Earth Syst. Sci., **11**(2), pp. 753–768.
[33] Bejan, A., and Merkx, G. W., 2007, *Constructal Theory of Social Dynamics*, Springer, New York.
[34] Lui, C. H., Fong, N. K., Lorente, S., Bejan, A., and Chow, W. K., 2012, "Constructal Design for Pedestrian Movement in Living Spaces: Evacuation Configurations," J. Appl. Phys., **111**(5), p. 054903.
[35] Reis, A. H., Miguel, A. F., and Aydin, M., 2004, "Constructal Theory of Flow Architectures of the Lungs," Med. Phys., **31**(5), pp. 1135–1140.
[36] Bejan, A., and Zane, J. P., 2013, *Design in Nature*, Anchor Books, New York.
[37] Bejan, A., 2016, *Physics of Life*, St. Martin's Press, New York.
[38] Cetkin, E., and Oliani, A., 2015, "The Natural Emergence of Asymmetric Tree-Shaped Pathways for Cooling of a Non-Uniformly Heated Domain," J. Appl. Phys., **118**(2), p. 024902.
[39] COMSOL, 2014, "COMSOL Multiphysics 5.0," COMSOL Inc., Burlington, MA.
[40] Bejan, A., and Lorente, S., 2008, *Design With Constructal Theory*, Wiley, Hoboken, NJ.
[41] Richter, J., 1970, *The Notebooks of Leonardo da Vinci*, Dover, New York.
[42] Minamino, R., and Tateno, M., 2014, "Tree Branching: Leonardo da Vinci's Rule Versus Biomechanical Models," PLoS One, **9**(4), p. e93535.